Magnetic Normal Modes of Bi-Component Permalloy Structures

GORGE GUBBIOTTI, Istituto Officina dei Materiali
PAM MALAGÒ, Dipartimento di Fisica e Geologia
STEVE FIN and STEVE RAM, Dipartimento di Fisica e Scienze
SOM TACCHI, Dipartimento di Fisica e Geologia
LAMP GIOVANNINI, Dipartimento di Fisica e Geologia
DAVID BISERO, Dipartimento di Fisica e Geologia
MIKE MADAMI, Dipartimento di Fisica e Geologia
GLEN CARLOTTI, Dipartimento di Fisica e Geologia

Two-dimensional[1] arrays of bi-component structures made of cobalt and permalloy elliptical dots with thickness of 25 nm, length 1 μm and width of 225 nm, have been prepared by a self-aligned shadow deposition technique. Brillouin light scattering has been exploited to study the frequency dependence of thermally excited magnetic eigenmodes on the intensity of the external magnetic field, applied along the easy axis of the elements.

CCS Concepts: • **Computer systems organization** → **Embedded systems**; *Redundancy*; Robotics; • **Networks** → Network reliability

General Terms: Design, Algorithms, Performance

Additional Key Words and Phrases: ACM proceedings, Word, text tagging

1 INTRODUCTION

In the last decade, there has been an intense research activity in studying the spectrum of magnetic eigenmodes both in single and multi-layered confined magnetic elements with different shape and lateral dimensions [1–8]. This interest has been further renewed by the emergence of the spin-transfer torque effect, where a spin-polarized current can drive microwave frequency dynamics of such magnetic elements into steady-state precessional oscillations. Moreover, the knowledge of the magnetic eigenmodes is very important also from a fundamental point of view for probing the intrinsic dynamic properties of the nanoparticles. It has been demonstrated that in MCs the spin wave dispersion is characterized by magnonic band gaps, i.e. frequency ranges where the spin wave propagation is not allowed. A peculiar feature of MCs with a complex base, i.e. where two dots or stripes of different shape or constituting materials form the basic unit cell, is that the magnetic order may not coincide with the geometrical one and, as a consequence, the dynamic response can be tuned in a reprogrammable way by varying the magnetic field strenght. A similar feature was already found in simple two-dimensional lattices with equal elements like, for example, in two or four-sublattice antiferromagnets and in two-sublattice antiferromagnets in the presence of a spin-flop transition. In addition to this, complex periodic arrays of dipolarly coupled magnetic dots are of special interest because they can support the propagation of non-reciprocal spin waves, i.e. $(\omega(k) \neq \omega(-k))$, where ω is the angular frequency and k is a wave vector, which could find application in the signal transmission and information processing as well as in the design of microwave isolators and circulators.

2 EXPERIMENTAL AND COMPUTATIONAL DETAILS

2.1 Sample Fabrication

Py/Co bi-component structures consisting of closely spaced (gap size d = 35 nm) elliptical dots of thickness 25 nm, length 1 μm and width 225 nm, respectively, dispersed in two different kinds of lattices, were fabricated by a self-aligned shadow deposition technique. Inter-dot distance along the chain of D = 140 nm while the inter-chain distance is D = 600 nm. The scanning electron microscopy image of the investigated bi-component sample, shown as inset of Fig. 1, reveals that the dots edge is quite sharp and far from that of an ideal ellipses.

Fig. 1. MOKE hysteresis loop for the bi-component Py/Co dots array measured along the dots long axis.

A reference sample consisting of an array of isolated bi-component elements with distance of 600 nm between the bi-component units in both the in-plane directions, was also patterned using the same technique and used to perform control experiment.

2.2 Quasi-Static Measurements: MOKE and MFM

2.2.1 Component Structures. Hysteresis loops were measured in the longitudinal configuration by magneto-optical Kerr effect (MOKE) using a Photo-Elastic Modulator operating at 50 kHz and lock-in amplification. The magnetic field, applied along the major axis of the elliptical elements, was swept between +1.0 and -1.0 kOe. To gain further information on the magnetization reversal process and the switching fields of the distinct dots, longitudinal minor loops were also measured.

2.2.2 Magnetization. To complement the above analysis of the magnetization evolution under an external field, the magnetic states of the bi-component structures were directly imaged at different point of the hysteresis cycle using in-field magnetic force microscopy (MFM) [5].

Eavesdropping. MFM images were recorded by a Digital Instruments Nanoscope IIIa, using the phase detection mode, i.e., monitoring the cantilever's phase of oscillation.

2.3 Dynamic Measurements: BLS

BLS spectra of the thermal magnetic excitations were measured at room temperature in the back-scattering geometry by using a (3+3)-pass tandem Fabry–Perot interferometer. About 200 mW of monochromatic (λ=532 nm) laser were focused onto a spot having a diameter of about 30 microns. An external magnetic field with intensity ranging between -1.0 kOe < H < +1.0 kOe was applied parallel to the sample surface along the dots length and perpendicular to the incidence plane of light (Voigt geometry).

Definition 3.1. A C-node is a set of live ranges (webs) in the AG or IG that are coalesced. Nodes within the same C-node cannot interfere with each other on the IG. Before any coalescing is done, each live range is a C-node by itself.

Lemma 3.4. *The solution to the C-MWPC problem is no worse than the solution to the MWPC.*

Proof. Simply, any solution to the MWPC is also a solution to the C-MWPC. But some solutions to C-MWPC may not apply to the MWPC (if any coalescing were made).

2.4 Ground-State Magnetization Determination and DMM Micromagnetic Simulations

2.4.1 Determined. The magnetization ground-states as well as the hysteresis loops were determined by using the OOMMF code. To reproduce the exact shape of the dots, a bitmap image of the basic unit of the bi-component dots was created from the SEM image of Fig. 1, and used as input for the simulations. Periodic boundary conditions have been applied to account for the chain arrangement of the Py/Co dots in the investigated sample.

2.4.2 Micromagnetic. For each micromagnetic cell the reduced magnetization takes the form where the magnetization (saturation magnetization) in the k-th cell; note that the saturation magnetization now depends on the ferromagnetic material through the index k. Hence, in a polar reference frame

$$(x + a)^n = \sum_{k=0}^{n} \binom{n}{k} x^k a^{n-k} \tag{1}$$

where K is the azimuthal (polar) angle of the magnetization (the time dependence is omitted). The second derivatives of the energy density depend on the micromagnetic cell indexes, and through them on the material index corresponding either to Py or Co. The expressions of E_{ext}, E_{exch}, E_{dmg} and E_{ani} are the same as the ones of the single-component system apart from the explicit dependence of the magnetic parameters on the given ferromagnetic material. Note that, unlike the bi-component system studied in Ref. 33, in the system studied here the inter-dot exchange contribution is set equal to zero, because in each unit cell the two elliptical dots are separated. Moreover, the uniaxial anisotropy energy density of Co is neglected.

> "Instead of using pairwise RTS/CTS frequency negotiation we propose lightweight frequency assignments, which are good choices for many deployed comparatively static WSNs. We develop new toggle transmission and snooping techniques to enable a single radio transceiver in a sensor device to achieve scalable performance, avoiding the nonscalable "one control channel + multiple data channels" design."

It is possible to write the following periodicity rule valid for the dynamic magnetization $\delta m(r)$ of each collective mode, a version of the Bloch theorem, viz. Note that, unlike the bi-component system studied in Ref. 33, in the system studied here the inter-dot exchange contribution is set equal to zero, because in each unit cell the two elliptical dots are separated. Moreover, the uniaxial anisotropy energy density of Co is neglected.

$$x = \frac{-b \pm \sqrt{b^2 - 4ac}}{2a} \tag{2}$$

Therefore one can observe either an in-phase (acoustic) or an out-of-phase (optical) character of the modes, with respect to the precession of the in-plane magnetization components in adjacent Py and Co dots.

Table 1. Frequency of Special Characters

Non-English or Math	Frequency	Comments
Ø	1 in 1,000	For Swedish names
$	4 in 5	Used in business[a]

Source: This is a table source note
[a]This is table footnote

1. Instead of using pairwise RTS/CTS frequency negotiation we propose lightweight frequency assignments, which are good choices for many deployed comparatively static WSNs.
2. We develop new toggle transmission and snooping techniques to enable a single radio transceiver in a sensor device to achieve scalable performance, avoiding the nonscalable "one control channel + multiple data channels" design.

We would like to mention that the DMM presents several advantages with respect to OOMMF for calculating the spectrum of magnetic eigenmodes for the following reasons: *a)* There is no need to excite the system by any magnetic field pulse, *b)* A single calculation llows to determine the frequencies and eigenvectors of all spin-wave modes of any symmetry, *c)* The spectrum is computed directly in the frequency domain, *d)* The mode degeneracy is successfully solved Table 1. The spatial profiles of the spin-wave modes are directly determined as eigenvectors and, finally, *f)* The differential scattering cross-section can be calculated accurately from the eigenvectors associated to each spin-wave mode.At point β (H= -372 Oe) of the hysteresis loop, where the plateau is observed in the *M-H* loop, the dark and bright spots of the Py dots are reversed with respect to those of Co, accounting for an antiparallel relative alignment of magnetization.

3 RESULTS AND DISCUSSION

3.1 Magnetization Curves and MFM Characterization

The major hysteresis loop measured by MOKE, plotted in Fig. 1, displays a two-step switching process due to the distinct magnetization reversal of the Py and Co sub-elements, characterized by a different coercivity. As the field is reduced from positive saturation (upper branch of the M-H loop), a 100% remanence is attained. On reversing the applied field, one observes a drop of the magnetization (between −240 and −370 Oe), proportional to the Py magnetization fraction within each bi-component unit (about 36%) in good agreement with experimental result (about 40%).

To directly visualize the evolution of the magnetization in the Py and Co subunits of our bi-component dots during the reversal process, we performed a field-dependent MFM analysis whose main results are reported in Fig. 2. At large positive field (H = +800 Oe, not shown here) and at remanence (α point of the hysteresis loop of Fig. 1), the structures are characterized by a strong dipolar contrast due to the stray fields emanated.

Fig. 2. MFM images of the bi-component Py/Co dots for different values of the applied magnetic field which are indicated by greek letters along both the major and minor hysteresis loop.

The Py and Co dots. This is a clear indication that both the Py and Co sub-elements are in a single domain state where Py and Co magnetizations are all oriented with their magnetic moment along of the chain where the plateau is observed in the *M-H* loop, the dark and bright spots of the Py dots are reversed with respect to those of Co, accounting for an antiparallel relative alignment of magnetization.

At relatively large negative fields (point γ, H = -770 Oe) the magnetization reversal is completed and the magnetization of the two adjacent sub-elements are saturated in the negative direction. The ground state remains unchanged when the field is now reduced to zero, i.e. remanent state coming from negative saturation, as confirmed by the MFM image taken at point δ of Fig. 1.

ALGORITHM 1: Iterative Algorithm

---

current_position ← *center*
current_direction ← *up*
current_position is inside circle
while *current_position* **is inside circle**, **do**
    neighborhood ← all grid hexes within two hexes from *current_position*
    for *each* hex *in* neighborhood, **do**
        for *each* neuron *in* hex **do**
            convert *neuron_orientation* to *vector*
            scale *vector* by *neuron_excitation*
            vector_sum ← *vector_sum* + *vector*
        end
    end
    normalize *vector_sum*
    current_position ← *current_position* + *vector_sum*
    current_direction ← *vector_sum*
    return *current_position*
end

We have also used MFM to measure the magnetic configurations along the minor hysteresis loop, described above. Once the AP ground state has been generated at H= -500 Oe, the applied field is increased in the positive direction. The MFM image taken at point α' of Fig. 2, remanent state of the minor loop (H=0), shows that the AP state is stable and remains

unchanged until the magnetic field is increased up to +300 Oe where the Py magnetization reverses its orientation and returns
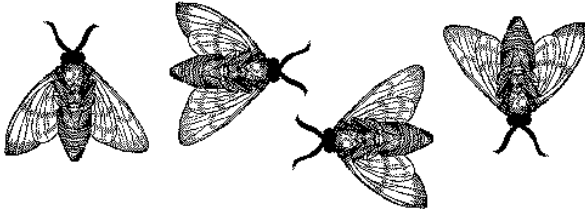

Fig. 3. Dependence of the magnetic eigeinmode wave frequency on the applied field strength.

to be aligned with that of Co dots. On the basis of the above MFM investigation, one can say that the structures are always in a single domain state.

3.2 Field Dependent BLS Measurements and DMM Calculations

Fig. 3 displays the frequencies of BLS peaks plotted as a function of the applied field magnitude starting from positive values. The field is then decreased and reversed following the upper branch of the hysteresis loop, shown in the same figure. Up to five peaks are measured in the spectra, as shown in spectrum measured at H=0 Oe in the Fig. 3 inset, and their field evolution analyzed over the whole field range investigated. The detected modes are identified and labeled on the basis of their calculated spatial profiles, shown in Fig. 4 for *H*= 500 and -500 Oe. They exhibit marked localization into either the Co or the Py dots, as stated at the end of the previous Section, were it was introduced the labelling notation containing the dominant localization region (either Py or Co) and the spatial symmetry (EM, F, DE, etc).

When the dots are in the P state, up to five modes were detected in BLS spectra. On the basis of the calculated profiles (right panel of Fig. 4), we identified in the P state the two modes at lowest frequencies as the EM(Py) and the F(Py), with a very small spin precession amplitude into the Co dot. This is because for this material we are below the frequency threshold for the existence of spin waves. A similar effect has been observed in periodic array of alternating Permalloy and Co nanostripes.

Note that the nodal lines present in the spatial profile of the F (Co) mode perpendicular to the long axis of the ellipse do not correspond to a real change of sign of the dynamic mode.
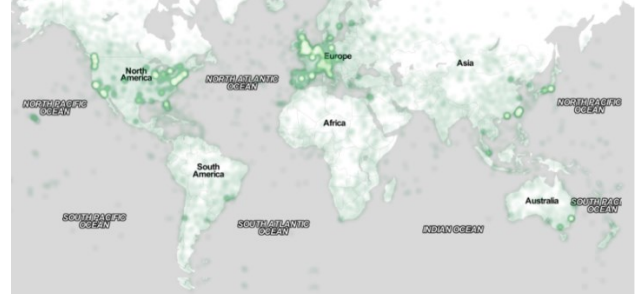

Fig. 4. Calculated spatial distribution of the in-plane dynamic magnetization.

Interestingly, the frequency slope of modes localized into the Co dots is larger than that of Py modes, due to larger values of the Co magnetization and gyromagnetic ratio. An overall good agreement between the calculated (dotted curves) and measured frequency (full points) has been achieved (see Fig. 3) even if some discrepancies are observed for the frequency of the EM and 1DE (Py) modes.

The corresponding spatial profiles of the modes are shown in the left panels of Fig. 4. Here one can see that the only mode which is purely localized in one dot is the EM of Co, because now it is sub-threshold for Py. A further reduction of *H*, which is sufficient to cause the Co magnetization reversal, produces a P state at negative fields and the frequency starts to increase again as a function of the applied field. In this field range the frequencies of modes in the Py dots monotonously increase in a way similar to that measured in the P state for positive field values while an abrupt change in the frequency of Co modes occurs.

Notice that if one stops increasing the negative field to about -300 Oe and comes back towards positive applied fields, BLS measurements can be performed following the minor hysteresis loop. This method permits to study, for example, the magnetization dynamics at remanence (without any external applied magnetic field) when the system is in the AP state (see MFM image α' in Fig. 2), a configuration which cannot be achieved at remanence along the major M-H loop. In Fig. 5 we show the modes frequency measured along the minor loop (full points) and compare them with values measured along the major M-H loop (open points).

By inspection of the frequency slope of the modes, one can immediately understand the localization of modes into dots of different materials looking at their slope.

In particular, for three (two) modes we measure a negative (Table 2) frequency slope with an almost linear dependence on *H*. It is evident that modes with negative frequency slope are modes localized into the Py dot (EM, F and 1DE) while the two with positive slope are the F(Co) and the EM(Co) modes.

Fig. 5. Full point are the frequencies measured along the minor hysteresis.

Table 2. Comparison of Coefficients from Atomistic

Atm	MS-CG	MS-CG/DPD
1.78	14.32	1.74 (-2%)
0.43	31.00	0.40 (-7%)
0.062	15.61	0.048 (-23%)
0.032	9.76	0.024 (-24%)
0.020	4.66	0.015 (-25%)
0.012	2.32	-"-
0.0076	0.016	-"-

Fig. 6. Calculated frequency evolution of modes detected in the BLS spectra.

3.3 Analysis of the Dynamic Coupling as a Function of the Gap Size

One interesting point which emerges from analysis of Figs. 3 and 4 is that the frequency values of the eigenmodes are not the same at +500 Oe and at -500 Oe. This is expected for modes localized into the Co elements, since the external field is either parallel or antiparallel to their magnetization. However, for those mode localized into the Py sub-element, one could have predicted to find the same frequency values at ±500 Oe, unless the dipolar coupling arising from the adjacent Co dot plays a significant role. In fact, as seen in Figs. 3 and 4, reversing the field from +500 to − 500 Oe, the frequencies of EM(Py) and 1DE(Py) modes increase by about 0.2 GHz and 0.6 GHz, respectively, while that of F(Py) decreases by 0.25 GHz. The reason of this complex behavior will be addressed in the following, analyzing the interplay of both static and dynamic dipolar coupling between the adjacent Py and Co dots. In Fig. 6 the calculated frequencies of the most representative eigenmodes at +500 Oe (FM state) and − 500 Oe (AP state) are plotted as a function of the gap size d between the Py and Co sub units (please remind that in the real sample studied here, d=35 nm). As

a general comment, it can be seen that the frequencies for the system in the AP state are more sensitive to d than those of the P state.

- In particular, the lowest three frequency modes of the AP state (EM(Co), EM(Py) and F(Py))
- Isolated elements (dotted lines) and show a marked decrease with reducing d, while the two modes at higher frequencies (F(Co) and 1DE(Py)).

4 CONCLUSIONS

In summary, we have performed both an experimental and theoretical study of the spin eigenmodes in dipolarly coupled bi-component cobalt and permalloy elliptical nanodots. Several eigenmodes have been identified and their frequency evolution as a function of the intensity of the applied magnetic field has been measured by Brillouin light scattering technique, encompassing the ground states where the cobalt and permalloy dots magnetizations are parallel or anti-parallel, respectively. In correspondence to the transition between the two different ground states, the mode frequency undergoes an abrupt variation and more than that, in the anti-parallelstate, the frequency is insensitive to the applied field strength. The experimental results have been successfully interpreted by the dynamic matrix method which permits to calculate both the mode frequencies and the spatial profiles.

A detailed micromagnetic investigation of the properties of the eigenmodes as a function of the gap distance between cobalt and permalloy elliptical dots has been performed and the consequent variation of the internal field has been calculated. It has been shown that the inter-dot dynamic dipolar coupling plays a crucial by affecting the spin-wave mode frequencies as a function of the gap size and induces a modulation of the corresponding spatial profiles both in cobalt and permalloy dots. We believe this work can stimulate conception, design and realization of reprogrammable magnonic crystals and microwave devices with improved performance basing on the magnetic contrast between different ferromagnetic materials.

A HEADINGS IN APPENDICES

The rules about hierarchical headings discussed above for the body of the article are di.erent in the appendices. In the appendix environment, the command section is used to indicate the start of each Appendix, with alphabetic order designation (i.e., the first is A, the second B, etc.) and a title (if you include one). So, if you need hierarchical structure within an Appendix, start with

subsection as the highest level. Here is an outline of the body of this document in Appendix-appropriate form:

REFERENCES

[1] Patricia S. Abril and Robert Plant. 2007. The patent holder's dilemma: Buy, sell, or troll? *Commun. ACM* 50, 1 (Jan. 2007), 36–44. DOI: http://dx.doi.org/10.1145/1188913.1188915

[2] I. F. Akyildiz, W. Su, Y. Sankarasubramaniam, and E. Cayirci. 2002. Wireless Sensor Networks: A Survey. *Comm. ACM* 38, 4 (2002), 393–422.

[3] David A. Anisi. 2003. *Optimal Motion Control of a Ground Vehicle.* Master's thesis. Royal Institute of Technology (KTH), Stockholm, Sweden.

[4] P. Bahl, R. Chancre, and J. Dungeon. 2004. SSCH: Slotted Seeded Channel Hopping for Capacity Improvement in IEEE 802.11 Ad-Hoc Wireless Networks. In *Proceeding of the 10th International Conference on Mobile Computing and Networking* (MobiCom'04). ACM, New York, NY, 112–117.

[5] Kenneth L. Clarkson. 1985. *Algorithms for Closest-Point Problems (Computational Geometry).* Ph.D. Dissertation. Stanford University, Palo Alto, CA. UMI Order Number: AAT 8506171.

[6] Jacques Cohen (Ed.). 1996. Special Issue: Digital Libraries. *Commun. ACM* 39, 11 (Nov. 1996).

[7] Bruce P. Douglass. 1998. Statecarts in use: structured analysis and object-orientation. In *Lectures on Embedded Systems*, Grzegorz Rozenberg and Frits W. Vaandrager (Eds.). Lecture Notes in Computer Science, Vol. 1494. Springer-Verlag, London, 368–394. DOI: http://dx.doi.org/10.1007/3-540-65193-429

[8] Ian Editor (Ed.). 2008. *The title of book two* (2nd. ed.). University of Chicago Press, Chicago, Chapter 100. DOI: http://dx.doi.org/10.1007/3-540-09237-4